Published on 06 July 2018. Downloaded by University of Science and Technology of China on 5/25/2021 8:55:44 AM.

Nanoscale

ROYAL SOCIETY OF CHEMISTRY

PAPER

View Article Online
View Journal | View Issue

Cite this: *Nanoscale*, 2018, **10**, 14885

Room-temperature ferroelectricity and a switchable diode effect in two-dimensional α-In_2Se_3 thin layers†

Siyuan Wan,[a] Yue Li,[a] Wei Li,[b] Xiaoyu Mao,[a] Wenguang Zhu*[a,b] and Hualing Zeng*[a,b]

Received 31st May 2018,
Accepted 5th July 2018

DOI: 10.1039/c8nr04422h

rsc.li/nanoscale

Nanoscale room-temperature ferroelectricity is ideal for developing advanced non-volatile high-density memories. However, reaching the thin film limit in conventional ferroelectrics is a long-standing challenge due to the presence of the critical thickness effect. van der Waals materials, thanks to their stable layered structure, saturated interfacial bonding and weak interlayer couplings, are promising for exploring ultra-thin two-dimensional (2D) ferroelectrics and device applications. Here, we demonstrate a switchable room-temperature ferroelectric diode built upon a 2D ferroelectric α-In_2Se_3 layer as thin as 5 nm in the form of a graphene/α-In_2Se_3 heterojunction. The intrinsic out-of-plane ferroelectricity of the α-In_2Se_3 thin layers is evidenced by the observation of reversible spontaneous electric polarization with a relatively low coercive electric field of ~2 × 10^5 V cm^{-1} and a typical ferroelectric domain size of around tens μm^2. Owing to the out-of-plane ferroelectricity of the α-In_2Se_3 layer, the Schottky barrier at the graphene/α-In_2Se_3 interface can be effectively tuned by switching the electric polarization with an applied voltage, leading to a pronounced switchable double diode effect with an on/off ratio of ~10^5. Our results offer a new way for developing novel nanoelectronic devices based on 2D ferroelectrics.

Introduction

Ferroelectrics, featured with reversible spontaneous electric polarization, play an important role in modern electronics with novel functionalities, such as high energy density capacitors,[1] resistive switches,[2–5] and non-volatile ferroelectric random-access memories (FERAMs).[6–8] Following the miniaturization of electronic devices, enormous effort has been devoted to exploring ultra-thin or nanoscale ferroelectrics with the goal of realizing 2D ferroelectricity.[9–16] However, the polarization instability in low-dimensional structures, for example the perovskite thin films,[10,12,17] results in a strong limitation on their applications in nanoelectronics. The origin of electric polarization vanishing below a critical size is complicated and still under debate.[18] A generally accepted explanation is the presence of a depolarization field in ultrathin ferroelectrics, which is due to the imperfect charge screening, local chemical environment, defects, and misfit strain at the interface.[10,12,13,17,19] Therefore, overcoming these obstacles and realizing a room-temperature stable ferroelectric phase in the thin film limit are crucial for future development of ferroelectric nanodevices.

With the innate stable layered structure and reduced surface energy, van der Waals (vdW) materials provide a versatile platform for studying 2D ferroelectricity at a single atomic layer limit. Previous studies[20–22] have confirmed the possibility of seeking a stable ferroelectric phase in layered materials with inversion symmetry breaking. For example, Chang *et al.*[21] reported the in-plane ferroelectricity in lattice distorted monolayer SnTe at a cryogenic temperature and Liu *et al.*[22] observed the out-of-plane electric polarization in 4 nm $CuInP_2S_6$ under ambient conditions. These pioneering findings inspire further study on layered 2D ferroelectrics. As a consensus, the practical application of ferroelectricity relies on three aspects: the technically more important out-of-plane electric polarization relative to the film plane, high ferroelectric transition temperature (T_c) and the simple lattice structure for materials realization. Based on these above findings, a recent theoretical predic-

[a] *International Center for Quantum Design of Functional Materials (ICQD), Hefei National Laboratory for Physical Science at the Microscale, and Synergetic Innovation Center of Quantum Information and Quantum Physics, University of Science and Technology of China, Hefei, Anhui 230026, China. E-mail: wgzhu@ustc.edu.cn, hlzeng@ustc.edu.cn*

[b] *Key Laboratory of Strongly-Coupled Quantum Matter Physics, Chinese Academy of Sciences, Department of Physics, University of Science and Technology of China, Hefei, Anhui 230026, China*

† Electronic supplementary information (ESI) available. See DOI: 10.1039/c8nr04422h

Published on 06 July 2018. Downloaded by University of Science and Technology of China on 5/25/2021 8:55:44 AM.

tion[23] of intrinsic room-temperature 2D ferroelectricity with both in-plane and out-of-plane electric polarization in a widely studied vdW material, α-In_2Se_3,[23–33] provides an ideal platform to explore the possibility of building novel 2D functional nanoelectronic devices.

Here, we report the observation of intrinsic out-of-plane ferroelectricity in α-In_2Se_3 thin layers and the demonstration of their practical ferroelectric device applications under ambient conditions. The Raman spectrum confirmed the crystal structure of ferroelectric In_2Se_3 thin layers to be the α phase, which is consistent with the previous theoretical prediction.[23] Using piezoresponse force microscopy (PFM), we reveal the existence of room-temperature spontaneous ferroelectric polarization in 5 nm α-In_2Se_3. The two antiparallel electric dipoles in the out-of-plane direction were clearly characterized using the PFM phase image with a contrast of 180°. The single-point poling measurements on samples of different thicknesses suggest a switchable out-of-plane electric polarization and a low coercive electric field in the order of 10^5 V cm^{-1} in α-In_2Se_3 thin layers. By applying an external electric field, we realize domain engineering with successful writing/erasing the polarity in a box-in-box pattern. Finally, as a demonstration of the device potential, we design and fabricate a ferroelectric diode in the graphene/α-In_2Se_3/few layer graphene (FLG) sandwich structure. The ferroelectric diode showed an on/off ratio of $\sim 10^5$. The current–voltage (I–V) hysteresis and a switchable diode effect have been observed. These findings in α-In_2Se_3 thin layers pave the way for developing novel 2D ferroelectric devices, such as non-volatile memories, high density capacitors, microelectromechanical systems (MEMS), and low power dissipation nanoelectronics.

Results and discussion

Crystal structure of α-In_2Se_3 thin layers

In_2Se_3 is a semiconducting vdW material with a direct band gap in the near infrared range.[25,29] It has been widely studied in the application of photodetectors,[25] phase-change memories,[29] and thermoelectric devices.[30] Despite intensive efforts, there are controversial identifications of its precise lattice structure between α and β phases.[25–28] Therefore, characterizing and analyzing the crystal structure of α-In_2Se_3 is necessary before studying its ferroelectric properties.

Fig. 1 presents the schematic crystal structure of layered α-In_2Se_3. In a unit cell, there are three quintuple layers (QLs), which follow the ABC stacking (3*R*) sequence *via* weak vdW interactions. From the point of view of lattice symmetry, α-In_2Se_3 is explicitly asymmetric in structure (as can be seen in Fig. 1a), fulfilling the prerequisite of inversion symmetry breaking in ferroelectrics. Each α-In_2Se_3 QL contains five single-element (In or Se) monolayers. These monolayers are stacked in a Se–In–Se–In–Se atomic layer sequence with strong covalent bonds. Within each In or Se atomic layer, the atoms form a triangular lattice. In an α-In_2Se_3 QL, the two outmost layers of Se atoms are both on the hollow sites of their neighboring layer of In atoms, with each Se atom being trigonally bonded to three In atoms and the same interlayer spacing. In contrast, the Se atoms in the middle layer are asymmetrically bonded to four In atoms from neighboring layers, constructing a tetrahedron structure with one vertical In–Se bond connected to one side and three In–Se bonds to the other side. As a consequence, there is a dramatic difference in the interlayer spacings between the middle Se layer and the two In layers, which produces net electric dipoles in the out-of-plane

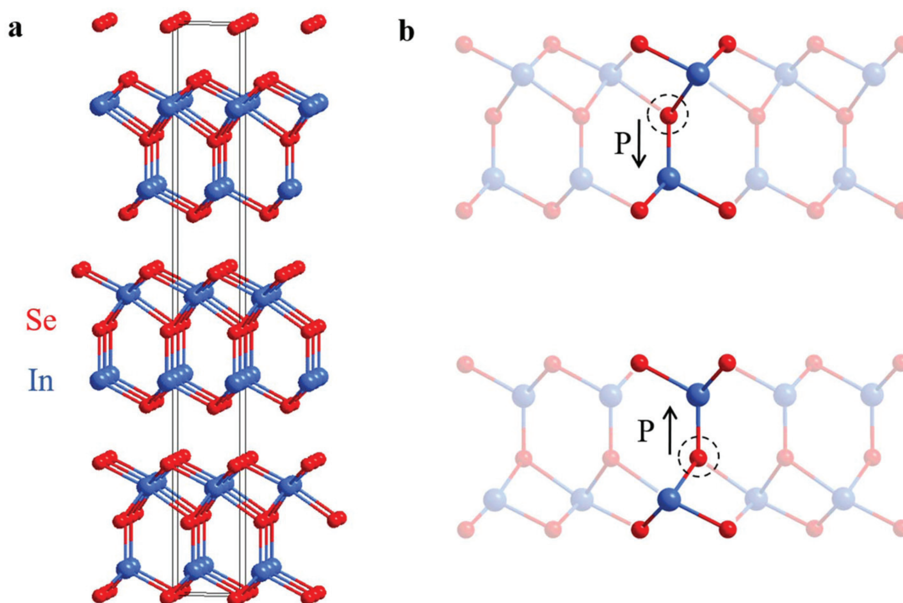

Fig. 1 Crystal structure of α-In_2Se_3. (a) Layer structure of α-In_2Se_3, with indium atoms and selenium atoms in blue and red, respectively. Each quintuple layer (QL) contains five atomic layers in the order of Se–In–Se–In–Se layers. Three QLs form a unit cell. (b) Side views of the two oppositely polarized structures of one QL α-In_2Se_3. The direction of spontaneous out-of-plane electric polarization is indicated by black arrows.

 This journal is © The Royal Society of Chemistry 2018

Published on 06 July 2018. Downloaded by University of Science and Technology of China on 5/25/2021 8:55:44 AM.

direction.[23] As shown in Fig. 1b, the out-of-plane ferroelectric polarization in α-In_2Se_3 has two degenerate states. The polarization direction, either upward or downward, is subjected to the atomic position deviation of the middle-layer Se atoms from the inversion center of the QL and thereby can be switched by applying an external electric field.

By knowing its origin of ferroelectricity, we start with materials realization (Fig. 2). The α-In_2Se_3 thin layers were prepared by the well-established mechanical exfoliation method from the bulk crystal (see the Experimental section). Fig. 2a shows a typical optical image of α-In_2Se_3 nanoflakes on the SiO_2/Si substrate with sharp optical contrast for different film thicknesses. Few-layer samples can be clearly visualized in the light/dark green area. The surface morphology and the sample thickness were further characterized by atomic force microscopy (AFM) in tapping mode under ambient conditions. As shown in Fig. 2b, the sample was atomically flat, indicating the characteristics of layered vdW materials. Some bright spots on the surface were residual polymers from the sticky tape during exfoliation. Fig. 2c shows the thickness profile measured along with the red dashed line in the sample topography image (Fig. 2b). The thinnest layer was found to be around 1.1 nm, which is close to the previously reported thickness for the α-In_2Se_3 monolayer (~1 nm).[27,28,34] To the best of our knowledge, it is the first successful demonstration of achieving high quality α-In_2Se_3 monolayers by the mechanical exfoliation method from bulk.

To confirm the crystalline structure of α-In_2Se_3 thin layers studied in this work, we characterize our samples with the Raman technique. Fig. 2d shows a typical Raman spectrum taken from a 50 nm α-In_2Se_3 thin layer with five dominant peaks. Similar Raman features were observed in thinner samples with a worse signal to noise ratio. According to the phonon dispersion of ferroelectric α-In_2Se_3 by density functional theory calculations,[23] the unique features of Raman active modes for α phase In_2Se_3 are the softening of the A_1 phonon mode (red shift if compared with the β phase due to the structure phase transition) and the distinct optical phonon at ~260 cm^{-1}. In our Raman spectrum, we observed the E symmetry mode at 89 cm^{-1} and the A_1(LO + TO) phonon mode at 104 cm^{-1}. By carefully checking the spectrum position of a similar mode from β-In_2Se_3 in previous studies,[29,35,36] centered at 110 cm^{-1}, we found that the observed A_1(LO + TO) phonon showed a slight red shift. In addition, two peaks centered at 180 cm^{-1} and 196 cm^{-1} were attributed to A_1(LO) and A_1(TO) modes, respectively, which were caused by the LO–TO splitting and confirmed the investigated In_2Se_3 to be asymmetric (belongs to the $R3m$ space group).[24] In particular, we also observed the distinct Raman feature at 266 cm^{-1}, which could be regarded as the determinant evidence for the crystal structure of ferroelectric α-In_2Se_3. The observed Raman features shown in Fig. 2d exclusively confirm the α phase crystal structure of In_2Se_3 thin layers studied in this work.

Ferroelectricity of α-In_2Se_3 thin layers

Ferroelectrics naturally possess a piezoelectric effect. Under an external electrical stimulus, the ferroelectric will deform either

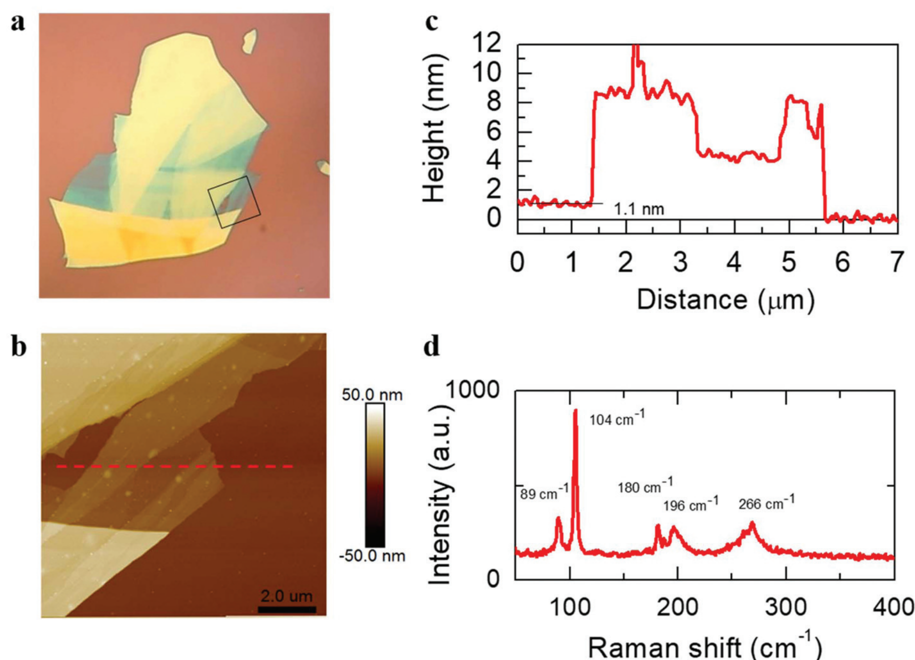

Fig. 2 Identification of α-In_2Se_3 thin layers. (a) Optical image of mechanically exfoliated α-In_2Se_3 thin layers on the SiO_2/Si substrate. (b) AFM topography (10 × 10 μm^2) of the zoomed area as squared in (a). (c) Corresponding height profiles taken along the red dashed line in (b). The thinnest film is 1.1 nm, close to the thickness of monolayer ~1 nm. (d) Raman spectrum of a 50 nm α-In_2Se_3 with 532 nm laser excitation. The four Raman peaks at 89, 104, 180 and 196 cm^{-1} are consistent with previous reports. The distinct Raman feature for ferroelectric α-In_2Se_3 is identified to be at 266 cm^{-1}.

Published on 06 July 2018. Downloaded by University of Science and Technology of China on 5/25/2021 8:55:44 AM.

in-phase (expand) or out-of-phase (contract) depending on the relative alignment between the polarization and the electric field (parallel or antiparallel). Therefore, piezoresponse force microscopy (PFM) is a versatile tool to study ferroelectricity. Fig. 3 shows the typical PFM measurements from few layer α-In_2Se_3 with a scanning area of 8 × 8 μm^2 under ambient conditions. The sample thickness was around 20 nm as shown in Fig. 3a. Spontaneous ferroelectric domains were directly visualized in the out-of-plane PFM phase image (Fig. 3b). By comparing the surface topography and the PFM phase image, we found that there was no correlation between the ferroelectric domain structures and the morphology, which eliminated the possible origin of the phase contrast contributed from the variation of the sample thickness. A 180° PFM phase contrast was observed, indicating the antiparallel ordering of electric dipoles in the out-of-plane direction between adjacent ferroelectric domains (Fig. 3c). The domain patterns were still discernible after several repeated measurements by PFM at room temperature. We also observed periodic ferroelectric stripe domains with a period of several nanometers in the as-exfoliated α-In_2Se_3 (Fig. S1, ESI†), which were commonly observed in $PbTiO_3$.[37–39] The antiparallel alignment of electric polarization between domains is the result of long-range electric dipole–dipole interactions with the lowest energy state as dictated by classical electrodynamics.

Another feature of ferroelectrics is the switch of the electric polarization direction under an external electric field. To check this, we carried out local electric polarization switching measurements by varying the bias on the sample with the conductive PFM tip and the heavily doped Si substrate. Fig. 3d and e show the out-of-plane amplitude (yellow) and the PFM phase (green) as a function of the applied electric field. Clear single and butterfly-like electric hysteresis loops were observed in the phase and the amplitude spectrum, respectively. The 180° reversal of the phase signal confirmed the characteristic switchable out-of-plane ferroelectric polarization in α-In_2Se_3 thin layers.[31] The strongly nonlinear bias-dependent behavior in the PFM amplitude spectrum excluded the tip–sample electrostatic effect.[40] In addition, the coercive field (E_c) of the α-In_2Se_3 thin layer was found to be around 200 kV cm^{-1} (Fig. S2, ESI†), which was far less than the reported value of 700 kV cm^{-1} for layered $CuInP_2S_6$.[22] The relatively low E_c in the α-In_2Se_3 thin layer implies superior applications in low-power 2D ferroelectric devices, such as the FERAMs. The measured PFM amplitude on ferroelectric domains allows the quantitative estimation of the longitudinal piezoelectric coefficient of the α-In_2Se_3 films. The piezoelectric coefficient d_{33}, which represents the electromechanical response of the α-In_2Se_3 thin layer in the c axis under an electric field in the same direction, can be estimated from

$$A = Qd_{33}V,$$

where A is the amplitude of the piezo force response under the applied voltage V and Q (~24) is the quality factor of the resonance for the cantilever used in the measurement (Fig. S3, ESI†). The piezoelectric coefficient d_{33} of 15 nm and 5 nm α-In_2Se_3 (Fig. S3a and b, ESI†) was estimated to be around 2 ± 0.28 pm V^{-1} and 1.17 ± 0.38 pm V^{-1}, respectively. However, it should be noted that due to the inhomogeneous distribution of the electric field at the PFM tip, there would be some error

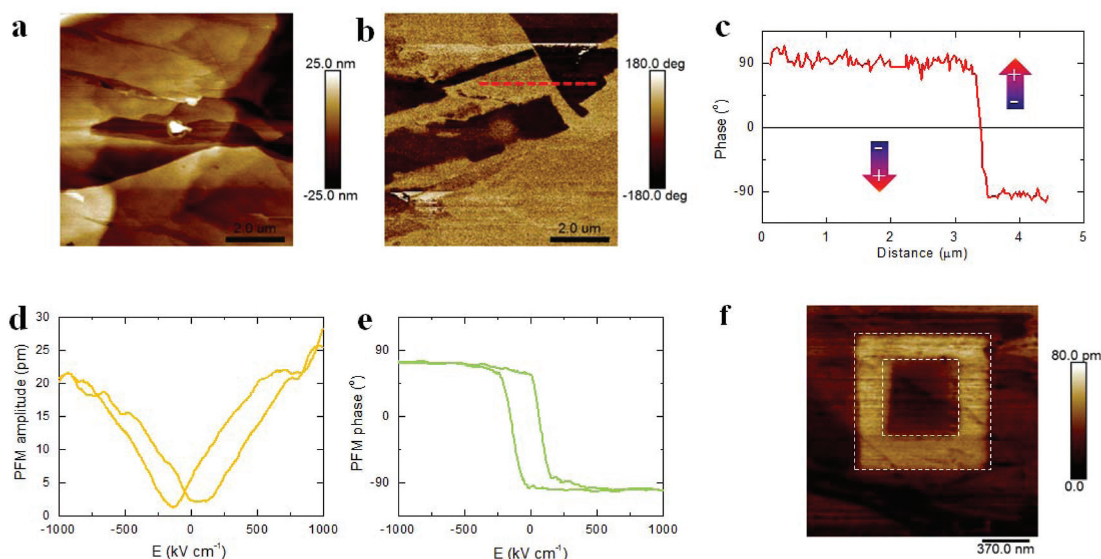

Fig. 3 Ferroelectricity of α-In_2Se_3 thin layers. (a) The surface topography of α-In_2Se_3 thin layers (~20 nm) on the heavily doped Si substrate. The scale bar is 2 μm. (b) The corresponding PFM phase image in the out-of-plane direction, showing clear ferroelectric domains. (c) The phase profile of different ferroelectric domains as sketched by the red dashed line in (b). A phase contrast of 180° is observed, which indicates the antiparallel directions of out-of-plane electric polarization between the adjacent domains. The arrows indicate the directions of electric polarization. (d) PFM amplitude and (e) PFM phase hysteresis loop measured from α-In_2Se_3 thin layers. (f) PFM amplitude image of domain engineering in α-In_2Se_3 with a film thickness of 12 nm. The scale bar is 370 nm.

 This journal is © The Royal Society of Chemistry 2018

Published on 06 July 2018. Downloaded by University of Science and Technology of China on 5/25/2021 8:55:44 AM.

in the estimation of the piezoelectric coefficient d_{33} from PFM measurements. We further performed control experiments on $BaTiO_3$, hBN and the doped Si substrate with the same technique (Fig. S4, ESI†). A clear electric hysteresis loop was found in $BaTiO_3$ (BTO) single-domain strained films on the $SrTiO_3$ substrate. The coercive field of 100 nm BTO was estimated to be 68 kV cm^{-1}, which was consistent with the literature.[41] The measurements from few-layer hBN and the heavily doped Si substrate showed paraelectricity without the electric hysteresis loop, which ruled out the possible charge accumulation effect at the interfaces in the PFM measurements of the α-In_2Se_3 thin layer.

To test the memory effect in ferroelectric α-In_2Se_3 thin layers, we artificially fabricated nanoscale ferroelectric domains with biased PFM tips. Fig. 3f shows a 1.8 × 1.8 μm^2 out-of-plane PFM amplitude image with an electrically written domain structure in α-In_2Se_3 thin layers of thickness down to 12 nm. The domain pattern was created by two steps. A 1 × 1 μm^2 area (denoted by a dashed-line frame in Fig. 3f) with either one of the two out-of-plane electric polarizations was firstly written under positive bias. Next, in the center, a small area of 0.5 × 0.5 μm^2 was rewritten or erased with a negative voltage. With these two steps, a box-in-box ferroelectric domain pattern was successfully created in the written/erased area. More importantly, there was no obvious damage to the surface morphology in the corresponding area after writing/erasing the electric polarization. The retention performance of the ferroelectric domains in the α-In_2Se_3 thin layer was found for more than 24 hours (details can be found in Fig. S6, ESI†).

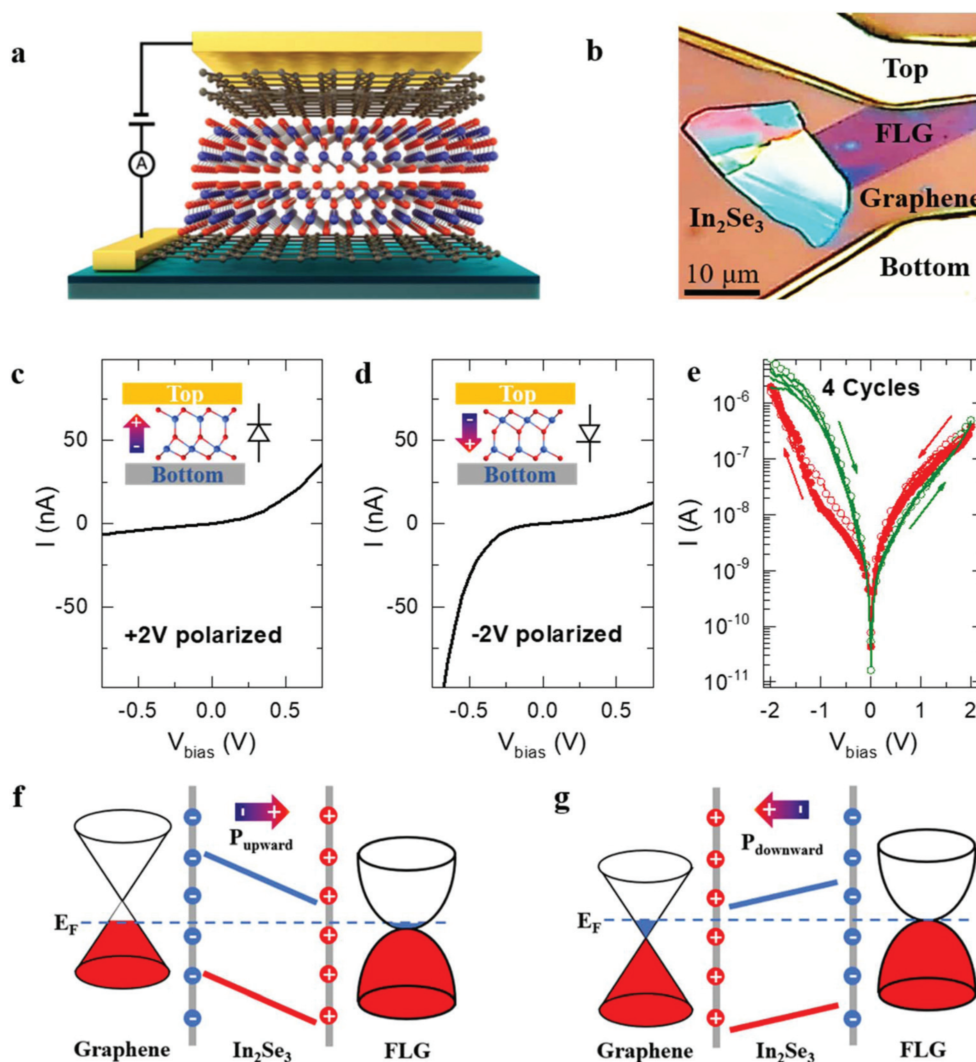

Fig. 4 Switchable ferroelectric diode based on α-In_2Se_3 thin layers. (a) Schematic and (b) optical image of the device. (c) and (d) *I*–*V* curves of the ferroelectric diode with switchable rectifying behavior. (e) *I*–*V* curves measured under high DC bias, showing clear hysteresis characteristics. The arrows indicate the voltage sweeping sequence. (f) and (g) Schematic of energy band diagrams of the graphene/In_2Se_3 heterostructure, illustrating the evolution of the Schottky barrier in the polarization state of the ferroelectric. The positive and negative charges on the vertical grey lines stand for the polarization charges on the top and bottom sides of the α-In_2Se_3 thin layer. The screening charges are visualized in the graphene/FLG electrodes.

View Article Online

Published on 06 July 2018. Downloaded by University of Science and Technology of China on 5/25/2021 8:55:44 AM.

Switchable ferroelectric diode based on α-In_2Se_3 thin layers

As a demonstration of its device potential, we design and build up a 2D ferroelectric diode with α-In_2Se_3 thin layers (thickness > 5 nm) (Fig. 4). In the ferroelectric diode, the α-In_2Se_3 thin layers are sandwiched by graphene with different thicknesses, monolayer and few-layer graphene as the bottom and top electrodes, respectively. The schematic device structure and the corresponding optical image of the device are shown in Fig. 4a and b. Typical *I–V* curves of the ferroelectric diode show characteristic rectifying behavior as shown in Fig. 4c and d. The diode-like rectifying effect is due to the formation of Schottky barriers (details are discussed in ESI Note 3, ESI†) within the two interfaces of our device (α-In_2Se_3/graphene and α-In_2Se_3/FLG).

Unlike conventional diodes, which conduct current in only one direction, the polarity of ferroelectric diodes can be switched by the polarization state of the α-In_2Se_3 thin layers. By applying DC bias at ±2 V, which was high enough to polarize the ferroelectric α-In_2Se_3 thin layer, we found that the rectifying behavior of the diode was switched. On polarizing with +2 V bias, the device showed forward rectifying behavior (Fig. 4c). In contrast, after applying −2 V bias, the diode was reversed, showing a backward rectifying effect (Fig. 4d). The unique switchable rectifying behavior of the ferroelectric diode is due to the modification of the Schottky barrier at the two interfaces by the following two aspects: (1) the generation of the reversible built-in electric field in the α-In_2Se_3 thin layer, which dramatically shifts the electronic bands with respect to the vacuum level on its two sides;[4,21] and (2) the different doping levels in the bottom and top graphene electrodes by the induced screening charges. The α-In_2Se_3 thin layers studied in this work are n-type. By considering the difference of its electron affinity and the working functions of top (intrinsic FLG) and bottom (p-type monolayer graphene) electrodes, we found that the Schottky barrier at the bottom α-In_2Se_3/graphene interface was much higher than that at the top α-In_2Se_3/FLG interface. As a result, the diode was originally conductive in the forward direction, from α-In_2Se_3 to the FLG electrode. Fig. 4f shows the energy band diagram of our device in an upward polarization state (+2 V polarizing) with zero bias. The electric polarization of the α-In_2Se_3 thin layers was upward (from bottom to top), producing a strong built-in electric field pointing from the FLG to monolayer graphene (downward). Thereby, the Schottky barrier at the graphene/α-In_2Se_3 interface was enhanced, while it slightly reduced in the top interface between α-In_2Se_3 and the FLG electrode, resulting in enhanced forward rectifying behavior of the ferroelectric diode. In the case of the −2 V polarized state, as seen from the band diagram in Fig. 4g, the built-in electric field was reversed. The graphene in the bottom was tuned to be n-type by the induced negative screening charges, while the Fermi level of FLG remains slightly changed. As a consequence, the Schottky barrier at the bottom graphene/α-In_2Se_3 interface was strongly suppressed if compared to the upward polarized state. The device functioned as a reverse (backward) diode.

We further studied the *I–V* characteristic of the ferroelectric diode under high DC bias. The *I–V* curves were obtained by sweeping the bias voltage from −2 V to +2 V and then backward to −2 V. The sweeping rate was maintained at a relatively low level to ensure the complete reversal of ferroelectric polarization. The *I–V* curves (Fig. 4e) show distinct hysteresis behavior, indicating the resistive switching effect.[4,42] Under high DC bias on both positive and negative sides, due to the modification of the Schottky barrier, the device is in its "on" state. The on/off ratio of the ferroelectric diode was found to be in the order of $\sim 10^5$. Notably, after dozens of electric polarization switching cycles, the ferroelectric diode sustains the hysteretic *I–V* characteristic (4 cycles are presented in Fig. 4e). Similar switchable rectifying behavior was found in a ferroelectric device with different structures, ultrathin α-In_2Se_3 (thickness ∼5 nm) sandwiched by graphene and metal (Al) electrodes (detailed in Fig. S7 and ESI Note 4, ESI†). The demonstration of the ferroelectric diode based on α-In_2Se_3 thin layers paves the way for developing novel 2D functional devices.

Conclusion

In summary, we have demonstrated room-temperature stable out-of-plane ferroelectricity in α-In_2Se_3 thin layers with a film thickness down to 5 nm. An external electric field can reverse the electric polarization and thereby modify the domain structure at the nanoscale. In the graphene/α-In_2Se_3 heterostructure, we find a switchable diode effect, showing controllable rectifying *I–V* behavior. The ferroelectric α-In_2Se_3 provides a new platform for developing novel two-dimensional functional devices as well as the possibility of integration with other vdW materials.

Methods

Sample preparation and device fabrication

Atomically thin α-In_2Se_3 and few-layer graphene were prepared by the mechanical exfoliation method from single crystal bulk samples onto silicon wafers with 300 nm thick SiO_2 on top. The samples were firstly visualized with interference color contrast through an optical microscope. Typical optical images can be found in Fig. 2a. The thickness was further confirmed by AFM (Bruker Dimension Icon) with tapping mode. The vdW heterostructures were stacked *via* the all-dry transfer technique.[43] The devices were fabricated by standard optical lithography, with the metal electrodes made by deposition of 10 nm titanium and 100 nm aluminum *via* an e-beam evaporator.

Raman spectroscopy and PFM measurements

Raman spectra were recorded using a Horiba Raman system (Labram HR Evolution) with 532 nm laser excitation. The on-sample power of the excitation was 100 μW. Piezoresponse force microscopy measurements were performed on a Bruker

This journal is © The Royal Society of Chemistry 2018

Published on 06 July 2018. Downloaded by University of Science and Technology of China on 5/25/2021 8:55:44 AM.

Dimension Icon with Ir/Pt conducting tips (Nanoworld) with 300 kHz excitation frequency under ambient conditions. The conductive substrates used were heavily doped silicon. A Keysight B2900 source meter was used to measure the *I–V* characteristics. During the sweeping process, the dwell time of every test point was 1 second to ensure the reversal of electric polarization.

Conflicts of interest

The authors declare no conflict of interest.

Acknowledgements

This work was supported by the National Key Research and Development Program of China (Grant No. 2017YFA0205004, 2017YFA0204904 and 2018YFA0306600), the National Natural Science Foundation of China (Grant No. 11674295, 11674299, 11374273, and 11634011), the Fundamental Research Funds for the Central Universities (Grant No. WK2340000082 and WK2060190084) and the China Government Youth 1000-Plan Talent Program. This work was partially carried out at the USTC Center for Micro and Nanoscale Research and Fabrication.

References

1 P. Kim, N. M. Doss, J. P. Tillotson, P. J. Hotchkiss, M.-J. Pan, S. R. Marder, J. Li, J. P. Calame and J. W. Perry, *ACS Nano*, 2009, **3**, 2581–2592.
2 M. Y. Zhuravlev, R. F. Sabirianov, S. S. Jaswal and E. Y. Tsymbal, *Phys. Rev. Lett.*, 2005, **94**, 246802.
3 V. Garcia, S. Fusil, K. Bouzehouane, S. Enouz-Vedrenne, N. D. Mathur, A. Barthélémy and M. Bibes, *Nature*, 2009, **460**, 81.
4 C. Wang, K.-J. Jin, Z.-T. Xu, L. Wang, C. Ge, H.-B. Lu, H.-Z. Guo, M. He and G.-Z. Yang, *Appl. Phys. Lett.*, 2011, **98**, 192901.
5 D. Pantel, S. Goetze, D. Hesse and M. Alexe, *ACS Nano*, 2011, **5**, 6032–6038.
6 J. F. Scott and C. A. Paz de Araujo, *Science*, 1989, **246**, 1400–1405.
7 M. Dawber, K. M. Rabe and J. F. Scott, *Rev. Mod. Phys.*, 2005, **77**, 1083–1130.
8 P. Sharma, Q. Zhang, D. Sando, C. H. Lei, Y. Liu, J. Li, V. Nagarajan and J. Seidel, *Sci. Adv.*, 2017, **3**, e1700512.
9 A. V. Bune, V. M. Fridkin, S. Ducharme, L. M. Blinov, S. P. Palto, A. V. Sorokin, S. G. Yudin and A. Zlatkin, *Nature*, 1998, **391**, 874.
10 M.-W. Chu, I. Szafraniak, R. Scholz, C. Harnagea, D. Hesse, M. Alexe and U. Gösele, *Nat. Mater.*, 2004, **3**, 87.
11 D. D. Fong, G. B. Stephenson, S. K. Streiffer, J. A. Eastman, O. Auciello, P. H. Fuoss and C. Thompson, *Science*, 2004, **304**, 1650–1653.
12 M. Stengel, D. Vanderbilt and N. A. Spaldin, *Nat. Mater.*, 2009, **8**, 392.
13 H. Lu, X. Liu, J. D. Burton, C. W. Bark, Y. Wang, Y. Zhang, D. J. Kim, A. Stamm, P. Lukashev, D. A. Felker, C. M. Folkman, P. Gao, M. S. Rzchowski, X. Q. Pan, C. B. Eom, E. Y. Tsymbal and A. Gruverman, *Adv. Mater.*, 2012, **24**, 1209–1216.
14 D. Lee, H. Lu, Y. Gu, S.-Y. Choi, S.-D. Li, S. Ryu, T. R. Paudel, K. Song, E. Mikheev, S. Lee, S. Stemmer, D. A. Tenne, S. H. Oh, E. Y. Tsymbal, X. Wu, L.-Q. Chen, A. Gruverman and C. B. Eom, *Science*, 2015, **349**, 1314–1317.
15 M. Wu and X. C. Zeng, *Nano Lett.*, 2016, **16**, 3236–3241.
16 W. Hua and Q. Xiaofeng, *2D Mater.*, 2017, **4**, 015042.
17 J. Junquera and P. Ghosez, *Nature*, 2003, **422**, 506.
18 P. Gao, Z. Zhang, M. Li, R. Ishikawa, B. Feng, H.-J. Liu, Y.-L. Huang, N. Shibata, X. Ma, S. Chen, J. Zhang, K. Liu, E.-G. Wang, D. Yu, L. Liao, Y.-H. Chu and Y. Ikuhara, *Nat. Commun.*, 2017, **8**, 15549.
19 C. Lichtensteiger, J.-M. Triscone, J. Junquera and P. Ghosez, *Phys. Rev. Lett.*, 2005, **94**, 047603.
20 A. Belianinov, Q. He, A. Dziaugys, P. Maksymovych, E. Eliseev, A. Borisevich, A. Morozovska, J. Banys, Y. Vysochanskii and S. V. Kalinin, *Nano Lett.*, 2015, **15**, 3808–3814.
21 K. Chang, J. Liu, H. Lin, N. Wang, K. Zhao, A. Zhang, F. Jin, Y. Zhong, X. Hu, W. Duan, Q. Zhang, L. Fu, Q.-K. Xue, X. Chen and S.-H. Ji, *Science*, 2016, **353**, 274–278.
22 F. Liu, L. You, K. L. Seyler, X. Li, P. Yu, J. Lin, X. Wang, J. Zhou, H. Wang, H. He, S. T. Pantelides, W. Zhou, P. Sharma, X. Xu, P. M. Ajayan, J. Wang and Z. Liu, *Nat. Commun.*, 2016, **7**, 12357.
23 W. Ding, J. Zhu, Z. Wang, Y. Gao, D. Xiao, Y. Gu, Z. Zhang and W. Zhu, *Nat. Commun.*, 2017, **8**, 14956.
24 R. Lewandowska, R. Bacewicz, J. Filipowicz and W. Paszkowicz, *Mater. Res. Bull.*, 2001, **36**, 2577–2583.
25 R. B. Jacobs-Gedrim, M. Shanmugam, N. Jain, C. A. Durcan, M. T. Murphy, T. M. Murray, R. J. Matyi, R. L. Moore and B. Yu, *ACS Nano*, 2014, **8**, 514–521.
26 X. Tao and Y. Gu, *Nano Lett.*, 2013, **13**, 3501–3505.
27 D. Wu, A. J. Pak, Y. Liu, Y. Zhou, X. Wu, Y. Zhu, M. Lin, Y. Han, Y. Ren, H. Peng, Y.-H. Tsai, G. S. Hwang and K. Lai, *Nano Lett.*, 2015, **15**, 8136–8140.
28 J. Zhou, Q. Zeng, D. Lv, L. Sun, L. Niu, W. Fu, F. Liu, Z. Shen, C. Jin and Z. Liu, *Nano Lett.*, 2015, **15**, 6400–6405.
29 Q. Wang, L. Yang, S. Zhou, X. Ye, Z. Wang, W. Zhu, M. D. McCluskey and Y. Gu, *J. Phys. Chem. Lett.*, 2017, **8**, 2887–2894.
30 G. Han, Z.-G. Chen, J. Drennan and J. Zou, *Small*, 2014, **10**, 2747–2765.
31 Y. Zhou, D. Wu, Y. Zhu, Y. Cho, Q. He, X. Yang, K. Herrera, Z. Chu, Y. Han, M. C. Downer, H. Peng and K. Lai, *Nano Lett.*, 2017, **17**, 5508–5513.
32 C. Cui, W.-J. Hu, X. Yan, C. Addiego, W. Gao, Y. Wang, Z. Wang, L. Li, Y. Cheng and P. Li, *Nano Lett.*, 2018, **18**, 1253–1258.

Published on 06 July 2018. Downloaded by University of Science and Technology of China on 5/25/2021 8:55:44 AM.

33 F. Xue, J. Zhang, W. Hu, W.-T. Hsu, A. Han, S.-F. Leung, J.-K. Huang, Y. Wan, S. Liu, J. Zhang, J.-H. He, W.-H. Chang, Z. L. Wang, X. Zhang and L.-J. Li, *ACS Nano*, 2018, **12**(5), 4976–4983.

34 M. Lin, D. Wu, Y. Zhou, W. Huang, W. Jiang, W. Zheng, S. Zhao, C. Jin, Y. Guo, H. Peng and Z. Liu, *J. Am. Chem. Soc.*, 2013, **135**, 13274–13277.

35 B. Nilanthy, R. S. Christopher, F. S. Emily, S. Jakub, G. Dean, W. M. Garry, M. Oleg, R. K. Zakhar, D. K. Zakhar, E. Laurence, P. Amalia and H. B. Peter, *2D Mater.*, 2016, **3**, 025030.

36 S. Zhou, X. Tao and Y. Gu, *J. Phys. Chem. C*, 2016, **120**, 4753–4758.

37 S. K. Streiffer, J. A. Eastman, D. D. Fong, C. Thompson, A. Munkholm, M. V. Ramana Murty, O. Auciello, G. R. Bai and G. B. Stephenson, *Phys. Rev. Lett.*, 2002, **89**, 067601.

38 C. M. Folkman, S. H. Baek, H. W. Jang, C. B. Eom, C. T. Nelson, X. Q. Pan, Y. L. Li, L. Q. Chen, A. Kumar, V. Gopalan and S. K. Streiffer, *Appl. Phys. Lett.*, 2009, **94**, 251911.

39 C. Thompson, D. D. Fong, R. V. Wang, F. Jiang, S. K. Streiffer, K. Latifi, J. A. Eastman, P. H. Fuoss and G. B. Stephenson, *Appl. Phys. Lett.*, 2008, **93**, 182901.

40 D. Seol, B. Kim and Y. Kim, *Curr. Appl. Phys.*, 2017, **17**, 661–674.

41 K. J. Choi, M. Biegalski, Y. L. Li, A. Sharan, J. Schubert, R. Uecker, P. Reiche, Y. B. Chen, X. Q. Pan, V. Gopalan, L.-Q. Chen, D. G. Schlom and C. B. Eom, *Science*, 2004, **306**, 1005–1009.

42 T. Choi, S. Lee, Y. J. Choi, V. Kiryukhin and S.-W. Cheong, *Science*, 2009, **324**, 63–66.

43 C.-G. Andres, B. Michele, M. Rianda, S. Vibhor, J. Laurens, S. J. v. d. Z. Herre and A. S. Gary, *2D Mater.*, 2014, **1**, 011002.

This journal is © The Royal Society of Chemistry 2018